*Clays and Clay Minerals*, Vol. 52, No. 2, 180–191, 2004.

# AN *IN SITU* TIME-RESOLVED XRD-PSD INVESTIGATION INTO Na-MONTMORILLONITE INTERLAYER AND PARTICLE REARRANGEMENT DURING DEHYDRATION

JAMES WILSON[1], JAVIER CUADROS[2,*] AND GORDON CRESSEY[2]

[1] Department of Earth Sciences, University of Bristol, Wills Memorial Building, Queen's Road, Bristol BS8 1RJ, UK
[2] Department of Mineralogy, The Natural History Museum, Cromwell Road, London SW7 5BD, UK

**Abstract**—X-ray diffraction with a position-sensitive detector (XRD-PSD) was used to make a time-resolved study of the dynamics of deposition and dehydration of Na-montmorillonite crystallites on flat substrates from deionized water suspensions. The static PSD geometry and simultaneous counting procedure allowed the acquisition of high-resolution data on the dynamics of interlayer and interparticle arrangements during dehydration. Three experimental datasets of Na-smectite dehydration are presented, each one representing different initial sample states (suspension, slurry and re-wetted thin film). The computer program NEWMOD was used to simulate one of the three datasets (dehydration of a smectite suspension) and thus obtain the apparent changes in relative proportions of different 00*l* values as smectite crystallites formed and dehydrated. Two types of diffracting domains formed: water-dispersed 'packets' of 1–2 smectite layers gaining long-range order in the *c* axis direction as water was lost to evaporation, and smectite layers deposited as hydrated crystallites with variable interlayer water contents. The experimental patterns show the rapid step-wise transition of Na-montmorillonite layers from *d* values of ~55 to 18.5, 15.4 and 12.5 Å, with variations that depended upon how the hydrated smectite sample was prepared. The simulations show that there was a wide range of *d* values whose frequency distribution changed as dehydration proceeded and that transient *d* values occurred between the peaks observed experimentally. The data obtained in this study illustrate that XRD-PSD instruments have great potential in providing detailed data on the rapid kinetics of interlayer reorganization.

**Key Words**—Dehydration, Position-sensitive Detector, Smectite, X-ray Diffraction.

## INTRODUCTION

Traditionally, the hydration state of smectite has been studied by means of XRD measurements of the positions of the 00*l* peaks and by gravimetric and thermogravimetric methods under controlled relative humidity conditions. It was noted by several workers that the basal spacing of smectite 2:1 layers appeared to increase with relative humidity in a step-wise fashion (Bradley *et al.,* 1937; Glaeser and Méring, 1968; MacEwan and Wilson, 1980), which approximately correlates with step-shape weight increase (Keren and Shainberg, 1975; Cases *et al.*, 1992). For the particular case of Na-smectite under low temperature and pressure conditions, it was observed that hydrated layers can possess 3, 2 or 1 'water-layer' systems (Glaeser and Méring, 1968; MacEwan and Wilson, 1980), with corresponding $d_{001}$ values of 18–19, 14.5–15.5 and 12.0–12.6 Å. The 18–19 Å smectite-water complex has been observed at relative humidity conditions approaching water saturation (Moore and Hower, 1986), the 14.5–15.5 Å hydration state occurs at approximately 60–90% relative humidity, and the 12.0–12.6 Å complex is observed under relative humidity conditions of up to ~60%. All water is lost and the layers collapse to 9.6 Å at 0% relative humidity.

* E-mail address of corresponding author:
j.cuadros@nhm.ac.uk
DOI: 10.1346/CCMN.2004.0520204

More recently, the atomic structure of hydrated smectite interlayers and its minimum energy configurations have been studied by computer simulation using molecular dynamics and Monte Carlo methods (*e.g.* Skipper *et al.*, 1991, 1995; Boek *et al.*, 1995a, 1995b; Chang *et al.*, 1995; Chatterjee *et al.*, 1999; Kawamura *et al.*, 1999; Sposito *et al.*, 1999). These studies confirm that the aforementioned hydration states of Na-smectite are energetically favored. They illustrate that with the step-wise increase in $d_{001}$ there is an increasing number of planes of maximum density of cations and water. However, these configurations do not represent simple stacked layers of hydrated cations.

Observations of slight variations in $d_{001}$ of the stable hydration configurations with varying humidity in Na-smectite led to the suggestion that smectite layers with different hydration states may be interstratified (MacEwan and Wilson, 1980). Moore and Hower (1986) reported the occurrence of regular interstratifications of 1-water layer and anhydrous Na-smectite layers, at relative humidity values from 65 to 12%. Cases *et al.* (1992) concluded that Na-smectite was a mixed-layer system of 0-, 1-, 2- and 3-water-layer hydrates, with the proportions of these hydrates varying under different relative humidity conditions.

The focus of this work is on the dynamics of transitions in the *c** layer repeat present in Na-montmorillonite crystallites as they form and undergo deposi-

tion and dehydration onto a flat substrate. This type of study requires fast data collection and a static beam-sample-detector geometry, which was achieved by using a diffractometer with a curved position-sensitive detector. Collins *et al.* (1992) also investigated the dynamics of smectite dehydration in their neutron diffraction study of the 001 reflections from Na- and Ca-exchanged smectite and vermiculite. However, their experimental conditions were different in that they used a water vapor-saturated atmosphere as the starting point of their experiments and then evacuated and heated the sample cell. In our study, additional information has been extracted from the results by modeling the experimental patterns with NEWMOD, which provides valuable information, especially in the water-dominated stages. DiMasi *et al.* (2001) recently analyzed the hydration state of a water-rich Na-smectite system using synchrotron X-ray radiation but their approach was static rather than dynamic. Interestingly, they found that the smectite layers settled in strata of different densities and orientations, with less dense and vertically oriented layers at the top of the column, and denser, horizontally oriented layers at the bottom. In this work, three experimental datasets of Na-smectite dehydration are presented, representing three different initial sample states: suspension, slurry and re-wetted thin film.

## METHODS AND MATERIALS

### *Position-sensitive detector X-ray diffractometry*

An Enraf-Nonius PDS 120 (Powder Diffraction System 120) X-ray diffractometer was used to characterize the material used in the experiments in addition to being used to investigate smectite dehydration. This instrument has a curved position-sensitive detector (PSD) spanning 120º2θ and fixed beam-sample-detector geometry, which enables the simultaneous acquisition of diffraction data at all angles within the detector range. Different static beam-sample incidence angles were used to optimize conditions for the following experiments: (1) phase quantification of the material used in the experiments; (2) smectite dehydration experiments with the beam at 'glancing-angle' incidence using a conventional X-ray source and (3) smectite dehydration experiments with the beam at 'glancing-angle' incidence using a high brightness Microsource X-ray generator. In all cases, the sample surface was rotated in its own plane during the acquisition of each diffraction pattern in order to maximize the number of crystallites in diffracting positions (Brindley, 1980).

The calibrants used for each experiment were the same, silver behenate ($C_{22}H_{44}O_2$·Ag; Blanton *et al.*, 1995) and silicon powder. Peak positions were measured at half-peak width at half height by fitting symmetric Pearson VII functions in the manner described by Howard and Preston (1989).

In the phase quantification experiment, a conventional sealed-tube X-ray source was operated under a potential of 45 kV with a beam current of 30 mA. A germanium crystal monochromator was used to select CuK$\alpha_1$ radiation from the primary beam. The beam dimension was constrained to be $0.24 \times 5.0$ mm by vertical and horizontal slits between the monochromator and sample. The angle of incidence of the beam to the sample surface was set at 5º.

For the dehydration experiment using a conventional sealed-tube X-ray source, a sequence of patterns was recorded, with each pattern having a counting time of 5 min. Each of these sequential diffraction patterns provided an averaged measurement or 'snapshot' of smectite-water rearrangements over the counting period. The angle of incidence of the beam on the sample was set at ~1º to allow diffraction from very low angles. The single-crystal silicon substrate upon which the sample was mounted also acted as a beam stop ensuring that no direct beam reached the detector window, resulting in a cut-off angle at 1.2º2θ in the diffraction patterns.

For the two dehydration experiments using a Microsource X-ray generator (manufactured by Bede Scientific Instruments Ltd), a CuKα beam consisting mainly of the $\alpha_1$ component was selected using a graphite crystal and a 0.5 mm pinhole aperture. The angle of incidence of the beam upon the sample surface was ~1º and gave a cut-off angle of 1º2θ. The waveguide used by the Microsource system gives a well collimated beam (almost parallel) that is more intense than the conventional sealed-tube X-ray source. Consequently, pattern collection times of only 60 s were used in these experiments. The software used with the diffractometer required 20 s to transfer the data to a computer. Therefore, a time-period of 80 s separated the onset of each subsequent pattern collection.

### *Smectite characterization*

The material used in this study was "Kunipia-F" (supplied by the Kunimine Industry Co. Ltd, Japan), which is a smectite-enriched fraction of the original bentonite rock. A near-random powder mount of Kunipia-F smectite was analyzed to identify the minerals present (Figure 1). The pattern was typical of dioctahedral smectite with 'turbostratic' disorder (Brindley, 1980) with trace amounts of quartz and cristobalite. Phase proportions were determined using the XRD-PSD method described by Batchelder and Cressey (1998), and yielded 97 wt.% smectite, 2 wt.% quartz and 1 wt.% cristobalite. Investigations by XRD-PSD of oriented air-dried and ethylene glycol-solvated mounts of this material were also conducted. Under a relative humidity of 38%, the $d_{001}$ of the air-dried material was 12.5 Å (typical of 1-water-layer Na-smectite, *e.g.* Glaeser and Méring, 1968; MacEwan and Wilson, 1980). The $d_{001}$ of the smectite after ethylene glycol solvation was 17 Å.

Major element concentrations were determined by X-ray fluorescence (XRF) spectrometric analysis of lithium metaborate glass beads using an energy dis-

https://doi.org/10.1346/CCMN.2004.0520204 Published online by Cambridge University Press

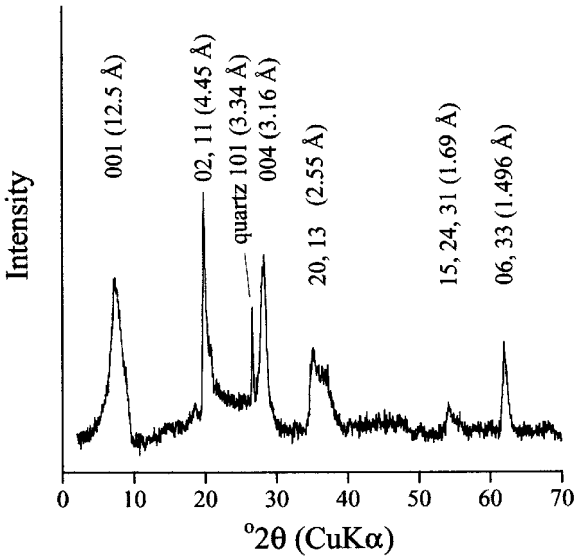


Figure 1. XRD-PSD pattern of a near-random powder mount of Kunipia-F smectite. The pattern was indexed using data given by Brindley (1980).

persive Spectro-Analytical X-Lab 2000 instrument. The Fe(II) content of the material was determined by digestion of samples in hot concentrated $H_2SO_4$ and HF in a Teflon vessel with subsequent complexing of HF with boric acid and titrating $K_2Cr_2O_7$ against dissolved Fe(II) with diphenylamine sulphonate indicator. The exchangeable cation content was determined on eight sub-samples using $Cu(EDA)_2^{2+}$ (Bergaya and Vayer, 1997). The supernatant fluids (which had near neutral pH values) from the $Cu(EDA)_2^{2+}$ exchange were acidified to 1% v/v $HNO_3$ and analyzed using inductively-coupled plasma atomic emission spectrometry (ICP-AES). An average total cation exchange capacity (CEC) of 135±3 meq/100 g was calculated.

After correction for the presence of quartz and cristobalite (subtraction of 3% wt. of $SiO_2$), the half unit-cell formula of Kunipia-F smectite was determined assuming tetrahedral Si+Al = 4. The interlayer cations from XRF and exchange analyses are in agreement. The calculated formula is:

$$(Na_{0.48}Ca_{0.03}K_{0.01})(Al_{1.54}Mg_{0.33}Fe^{3+}_{0.09}Fe^{2+}_{0.02})(Si_{3.87}Al_{0.13})\ O_{10}(OH)_2 \cdot nH_2O$$

*Experimental procedures*

Experiments were conducted using both Na-washed and untreated samples of Kunipia-F smectite. No differences in behavior were observed between the treated and untreated smectite. Three datasets are presented in this work, each one representing different sample preparation. In dataset 1, a suspension of smectite powder in deionized water was dispensed onto a flat single-crystal silicon substrate under atmospheric conditions of 47% relative humidity and 22ºC. X-ray diffraction patterns were collected, each for a 5 min duration, as dehydration proceeded. In dataset 2, smectite powder was wetted with several droplets of deionized water, then smeared as a thick slurry across a single-crystal quartz substrate and analyzed at 30% relative humidity and 25ºC. In dataset 3, a smectite suspension in deionized water was dispensed onto a single-crystal quartz substrate and allowed to dry to produce a well oriented thin film. Immediately prior to collecting the X-ray patterns, this film was re-wetted without dispersing the smectite with just enough deionized water to create a wet film. This dataset was collected at 28% relative humidity and 25ºC. Dataset 1 was recorded using a conventional sealed-tube X-ray source with a counting time of 5 min per pattern. Datasets 2 and 3 were collected using the Microsource™ X-ray source, with a collection time of 60 s for each successive pattern and a 20 s interval between patterns.

*NEWMOD simulations*

Five patterns from dataset 1 (dehydration of a suspension) representing key hydration states were simulated using the computer programme NEWMOD. This programme allows calculation of 00*l* profiles for end-members and mixed-layer phyllosilicates with different interlayer complexes. The programme and examples of its use are described by Reynolds and Reynolds (1996) and Moore and Reynolds (1997). NEWMOD was written to model patterns from scanning diffractometers but there is no essential impediment in using it to model XRD-PSD patterns. The patterns of oriented mounts generated with these two types of geometry are similar if the incidence angle used with the PSD diffractometer is not set at, or near to, any Bragg angle for the material of interest, since this would enhance the corresponding reflection with respect to the others. The incidence angle in these experiments of 1° means that only reflections near this angle are enhanced.

In the PSD geometry, where the angle between incident beam and sample surface remains constant, the series of diffraction orders are produced by different particles, according to their different orientations. In an oriented mount all particles tend to be near-parallel to the sample substrate and the abundance of particles lying at a specific angle from the substrate are expected to decrease as the angle increases. This means that the intensities of the 00*l* peaks are likely to decrease with increasing angles compared to a pattern from an oriented mount using a scanning X-ray diffractometer. Comparison of the patterns in this work with experimental patterns of Na-smectite from scanning diffractometers showed that the peak intensity ratio 001/00*n* ($n > 1$) in this work is the same for 001/002 and ~20% higher for 001/004. This is the only appreciable difference between our patterns and other Na-smectite patterns in the literature. The patterns in this work show

up to the 006 reflection of air-dried Na-smectite, indicating that there were smectite crystallites, or parts of them (*e.g.* curled ends) at angles of ~45º from the substrate. NEWMOD uses a default range of particle orientation with respect to the substrate of $\sigma^* = 12º$, where $\sigma^*$ is the standard deviation from a 0º angle in a Gaussian distribution. NEWMOD patterns calculated in these conditions show that even the 001/002 intensity ratio is lower than that of the patterns in this work. This is in agreement with the wider range of particle orientation in the dehydration experiments presented here.

The simulated smectite had no octahedral Fe and was saturated with $Na^+$. The chemical analysis indicated that the smectite has 0.11 Fe atoms per $O_{10}(OH)_2$. However, patterns calculated with 0 and 0.11 Fe atoms per $O_{10}(OH)_2$ were not significantly different.

The aim of the modeling was to characterize the diffracting units occurring during the dehydration process and to determine their apparent relative abundance. Two types of units were modeled: (1) particles dispersed in water and (2) particles deposited onto the sample substrate forming a well-oriented sample component. These units were characterized by different thicknesses of the coherently diffracting domain (in the *c* axis direction) and by different possible angles between the 2:1 layers and the sample substrate. Water-dispersed particles were considered to consist of single layers or two-layer 'packets' and to have a wide range of orientations that decreased with decreasing water content in the sample. Here, one layer represents one diffracting unit, *i.e.* two 2:1 units are necessary to create one layer, three 2:1 units to create 2 layers, *etc.* It is impossible to know the real range of particle orientations and the values given are only assumed. This affects the relative intensities of reflections and, in conjunction with the possible enhancement of those reflections near 1º (if there is a majority of layers near-parallel to the substrate), results in the inability to determine exactly the relative number of particles in different hydration states along the dehydration series. Instead, the simulations produced in this study give a coherent model of the approximate values of the changing relative proportions of particles in different hydration states during the course of the experiment. The most accurate relative proportions are those between crystallites of different $d_{001}$ values deposited onto the sample substrate because their 001 peaks are far from the intensity enhancement region at very low angle, their º2θ positions are close together and it is likely that their orientations were very similar. Only the 001 peaks were used to match the intensities of calculated and experimental patterns for this component of the sample. For the sedimented particles, the range of particle orientation with respect to the sample substrate was defined by $\sigma^* = 12º$, which is lower than the experimental one, as shown above, but this does not affect the calculations because all sedimented particles were simulated having the same orientation. The thickness of the diffraction domains of deposited particles was modeled by first estimating the mean thickness from the experimental patterns using the Scherrer equation, and then creating a log normal distribution of domain thickness with NEWMOD, from 1 to *N* layers per domain, in which *N* was obtained by best match with the experimental patterns. The mean value in the distribution is that obtained from the experimental patterns.

The experimental patterns that were simulated had a variable background at low angles (<5º2θ). NEWMOD simulations had a higher background than the corresponding patterns. To reduce the background to the correct intensity, a background curve was simulated using NEWMOD and subtracted from the calculated patterns. Calculated background curves were different for each of the calculated patterns because the different distributions of *d* values, coherent scattering domains and particle orientation generated different background shapes.

## RESULTS

### *Dataset 1: dehydration of a suspension of Na-smectite*

The 3-dimensional sequence plot of diffraction patterns of each of the three datasets are presented in Figure 2. For comparative purposes, 2-dimensional plots of XRD patterns from dataset 1 are given in Figure 3. There was abundant water on the substrate during the collection of the first few XRD patterns obtained in dataset 1 and they are dominated by two broad features, a dome-shaped maximum centered on ~25 Å (~3º2θ) caused by dispersed smectite layers, and a broader feature stretching from 15 to 60º2θ caused by diffuse (non-Bragg) X-ray scattering from water. In addition, a low-intensity smectite 02, 11 reflection was observed at ~20º2θ. As dehydration progressed, the intensity of the water scattering decreased and the broad smectite diffraction feature underwent several changes. The maximum moved to ~48 Å in the 20–25 min pattern, then it moved to ~35 Å in the 30–35 min pattern where it was only just apparent on the rising background (Figure 3). In the next pattern, it moved to ~65 Å, with a final shift to ~40 Å in the 50–55 min pattern, where it was last observed. This diffraction feature became narrower during the dehydration sequence (although not constantly) and its intensity increased in the 45–50 min pattern and decreased in the subsequent pattern.

In the middle of the dehydration sequence, there was a pronounced elevation of the background in the very low-angle region. This is caused by total external reflection (not a Bragg 'reflection') of part of the X-ray beam from the water surface and suspended clay crystallites because, at some point during evaporation, the angle between the surface of the water meniscus and

https://doi.org/10.1346/CCMN.2004.0520204 Published online by Cambridge University Press

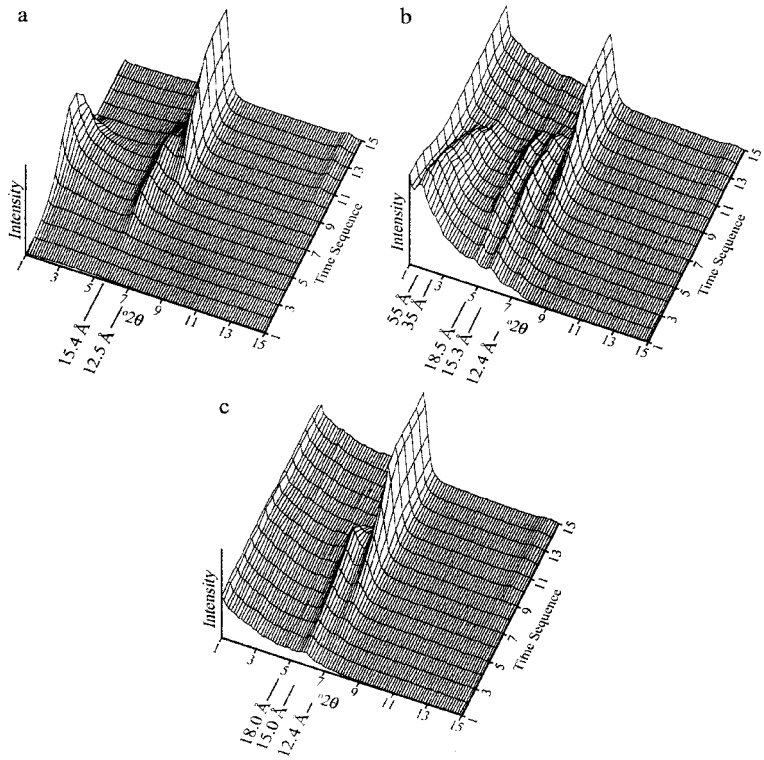


Figure 2. Three-dimensional plots of Na-smectite dehydration. a, b and c show datasets 1, 2 and 3, respectively. For dataset 1, each pattern was collected for 5 min. In datasets 2 and 3, counting time was reduced to 60 s per pattern.

the incident beam (or part of it) became <~0.2°, which is the critical angle for total reflection. This reflection feature could be reproduced by placing either only water or other mineral suspensions on the substrate, with the only difference being in the intensity of the background elevation. This effect was only seen in dataset 1, because it was the only experiment where a water meniscus was present. In the pattern simulations, this background elevation was treated as part of the overall pattern background.

The 001 peak for smectite with a 2-water-layer complex with *d* value of 15.4 Å (5.7°2θ) appeared after 15 min and grew in intensity, together with the corresponding 003 (5.14 Å, 17.53°2θ) and 005 (3.08 Å, 28.99°2θ) reflections. Then, the 001 (12.5 Å, 7.07°2θ), 002 (6.24 Å, 14.19°2θ) and 004 (3.12 Å, 28.61°2θ) reflections of smectite with a 1-water-layer complex appeared and coexisted with the higher hydration state for some time. Subsequently, the 00*l* peaks corresponding to the 15.4 Å structure decreased in intensity and disappeared while the 00*l* peaks corresponding to the 12.5 Å structure grew in intensity. The 00*l* series of these two hydration states showed rational values and, therefore, no appreciable mixed-layering of hydration states was present. The 001 peaks showed an apparent change in position that was not observed for higher-order peaks. The 15.4 Å peak moved from 15.7 Å (15–20 min) to 15 Å (40–45 min) and the 12.5 Å peak shifted from 12.7 Å (35–40 min) to 12.5 Å (70–75 min). This effect is due to changes in background intensity and the presence of other 001 peaks nearby. The 15.4 and 12.5 Å reflections were very sharp. As estimated with the Scherrer equation, their corresponding average diffraction domains along the *c** axis, in the 25–30 and 70–75 min patterns, were 128 and 183 Å, which corresponds approximately to 8 and 16 layers. This shows that the sedimentation of layers from suspension produced long-range-ordered units of relatively thick crystallites.

*Dataset 2: dehydration of a slurry of Na-smectite*

The backgrounds of the XRD patterns of datasets 2 and 3 were seen to increase with decreasing angle in the low°2θ region, but remained approximately constant in intensity throughout the dehydration experiments, in contrast to dataset 1 (suspension experiment). The higher overall background in datasets 2 and 3 is the result of using a slightly smaller beam-sample incidence angle and a different beam shape and cross-section (see methods).

Some of the detailed features described here for datasets 2 and 3 are not evident in Figure 2. The dehydrating slurry (dataset 2) showed a maximum at ~55 Å from the start of the experiment, which moved towards 35 Å and then decreased in intensity and disappeared as dehydration proceeded. This maximum

https://doi.org/10.1346/CCMN.2004.0520204 Published online by Cambridge University Press

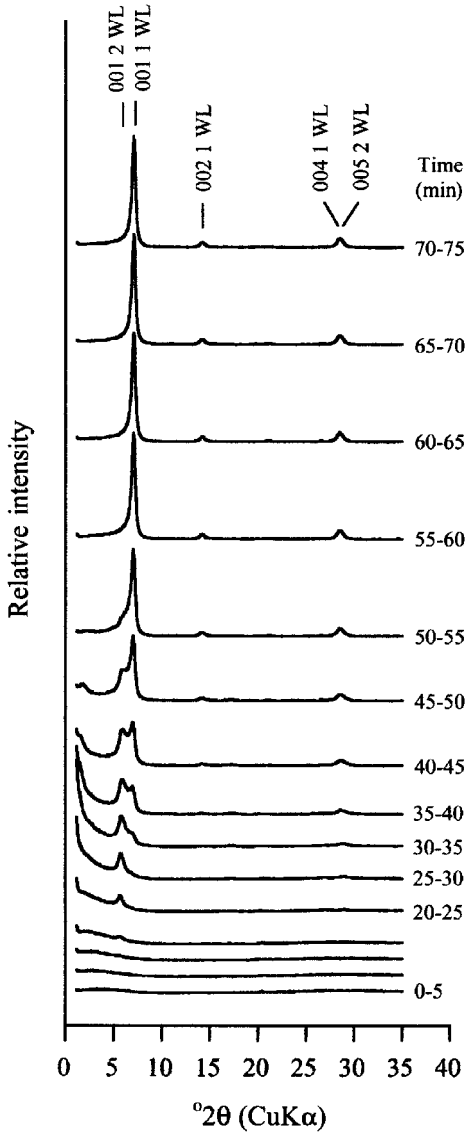


Figure 3. XRD patterns of Na-smectite dehydration (dataset 1). 00*l* peaks corresponding to interlayer structures with 2-water layers (2WL) and 1-water layer (1WL) are indicated.

is very similar to that in the 45–50 min pattern in the suspension experiment (dataset 1). From the beginning, two low-intensity peaks were present at 18.5 and 15.3 Å, corresponding to smectite with 3- and 2-water-layer complexes in the interlayer (Figure 2b). Initially, the two peaks increased in intensity, but then decreased and disappeared as the reflection corresponding to a 1-water-layer complex at 12.4 Å grew. For an 8 min period, during the central stages of the experiment, the four maxima coexisted. The main feature that differentiates this dataset from the others, is the stabilization of the 3-water-layer complex (18.5 Å). This complex persisted for as long as the 2-water-layer complex, although its intensity was lower and decreased more rapidly as dehydration proceeded. In spite of this loss of intensity, there was still a low-intensity residual 18.5 Å diffraction feature at the end of the experiment.

The high-order 00*l* peaks were broad and their *d* values were not completely rational. The 005 peak of the 15.3 Å structure appeared from the onset of the experiment at 3.07 Å. The 002 peak of the 12.4 Å complex was observed at 6.16 Å from pattern number 9 onwards and the corresponding 004 reflection appeared at 3.12–3.13 Å, although this overlaps with the 005 peak of the 15.3 Å structure and it is difficult to determine its exact position. The final 004 reflection at 3.12–3.13 Å was broad and asymmetric, with a shoulder toward the high-angle side. There was an apparent slight drift of the 001 peaks throughout the dehydration, similar to that observed in the suspension dataset and, as before, was due to peak overlap. The 001 peaks were broader than those given by the suspension experiment (dataset 1). The Scherrer average diffraction domain thickness estimated from the 12.4 Å peak at the end of the experiment was 149 Å (~12 layers).

### *Dataset 3: dehydration of a re-wetted powder film of Na-smectite*

The only two prominent maxima in this dataset were those from 2- and 1-water-layer complexes, which appeared sequentially as in the other datasets. However, broad, low-intensity maxima were present around 55, 35 and 18 Å in the patterns collected at the beginning of the experiment (not observable in Figure 2), although the 18 Å peak persisted in later patterns. The only high-order peaks observed clearly correspond to the 12.4 Å complex. These reflections did not seem to be completely rational and were quite broad (especially the 004 peak). The 002 peak had a *d* value of 6.17 Å, while the 004 peak had a *d* value of 3.12–3.13 Å. As in the previous datasets, there was a slight shift in the positions of the 001 peaks to higher angles which was not observed in the other 00*l* peaks. This is due to changes in background intensity and peak overlap as in the previous experiments.

### *NEWMOD simulation of dataset 1 (suspension)*

The calculated patterns simulated the presence of two types of particles: those dispersed in the water and those sedimented on the substrate. The parameters used in the calculations are shown in Table 1. The water-dispersed particles are individual layers or 2-layer 'packets' with variable orientation with respect to the sample substrate ($\sigma^*$ in Table 1). This orientation range decreases with time as water evaporates. The layers have different *d* values (Table 1), distributed over large ranges. The distribution of *d* values in the water-dispersed particles was simulated by creating patterns corresponding to random mixed-layer assemblages of two components (*e.g.* 18 Å/16 Å, 20 Å/18 Å, *etc.*). These patterns were then added together in varying proportions to provide a best-fit to the experimental patterns. The overall pattern

https://doi.org/10.1346/CCMN.2004.0520204 Published online by Cambridge University Press

Table 1. Parameters used in the calculated patterns.

| Pattern | *d* values (Å) | σ* (°)[1] | $N_{min}$[2] | $N_{max}$[3] | $N_{av}$[4] |
|---|---|---|---|---|---|
| 0–5 min | 12–55 | 90 | 1 | 2 | 1 |
| 25–30 min | 20–45 | 70 | 1 | 2 | 1 |
| | 15.42 | 12 | 1 | 10 | 8 |
| 40–45 min | 35–60 | 60 | 1 | 2 | 1 |
| | 15.3 | 12 | 1 | 10 | 8 |
| | 13.6 | 12 | 1 | 7 | 5 |
| | 12.46 | 12 | 1 | 13 | 10 |
| 45–50 min | 35–55 | 20 | 1 | 2 | 1 |
| | 15.3 | 12 | 1 | 10 | 8 |
| | 13.6 | 12 | 1 | 7 | 5 |
| | 12.46 | 12 | 1 | 14 | 12 |
| 70–75 min | 12.46 | 12 | 1 | 19 | 16 |

[1] Standard deviation of particle orientation with respect to sample substrate.
[2, 3, 4] Minimum, maximum and average number of smectite layers in the distribution of coherent scattering domain thicknesses

simulates the real behavior of smectite in the experiment, where water-dispersed layers gradually come into register with each other as they are deposited on the sample substrate. For simplicity, only the total ranges of *d* values of water-dispersed particles are shown in Table 1. The sedimented particles were considered to have a constant range of orientation with respect to the substrate and their *d* values and coherent scattering domain sizes were obtained by best-fit with the experimental patterns.

The results of the simulations are in good agreement with the experimental patterns (Figure 4). In the 0–5 and 25–30 min traces, the discrepancies (from 15°2θ) are due to X-ray scattering from the water, which was not simulated. In the 45–50 min pattern, there is a discrepancy at ~5°2θ. The higher intensity of the calculated pattern is caused by the 002 reflections of the packets generating the low-angle maximum at 55 Å (1.6°2θ). It was impossible to simulate this maximum with a limited number of components without also generating 002 reflections of significant intensity. It is likely that a perfect match could be obtained using a greater number of mixed-layer systems and variable particle orientation, but this would require a much more complicated simulation. Finally, small differences can also be observed in the intensity of the 00*l* reflections where $l > 1$. This is caused by the difference between PSD (experimental) and scanner (simulated) diffractometer beam-sample geometries, as discussed in the methods section.

The simulated XRD patterns allowed the apparent relative proportions of domains with a given layer spacing to be determined (Figure 5). Proportions are given for the two types of diffraction domain: water-dispersed 'packets' (filled circles) and deposited crystallites (open circles). The simulation shows that for between 0 and 5 min, there was a large range of *d* values or separations between layers, which decreased in number from ~12 to 55 Å (Figure 5). In the 25–30 min pattern, the distribution of *d* values between dispersed layers became narrower and changed shape, to give a maximum at ~25 Å. By this time, a few layers had been deposited onto the substrate which generated the 15.4 Å reflection. After 40 min, the simulations show that most particles had been deposited onto the substrate (open circles). The two observed 001 maxima were modeled by incorporating three components with *d* values of 12.5, 13.6 and 15.3 Å. The requirement of three $d_{001}$ values in the simulations shows that transient layer spacings existed between the 2- and 1-water-layer complexes as dehydration proceeded. The relative proportion of 12.5 Å layers increased at the expense of 15.3 and 13.6 Å layers as water evaporated. In Figure 5, the dots corresponding to water-dispersed and sedimented particles (crystallites with long-range order) are linked by a dashed line to indicate that their relative proportions are not quantitative given that the orientation distribution of the water-dispersed particles is unknown (as discussed in the methods section). However, it should be noted that the simulations did not produce good fits when particles with *d* values between 15.5 and 35 Å were included. The last pattern in Figure 4 shows the final stage of the dehydration process (at 47% relative humidity), where Na-smectite has an homogeneous hydration state, corresponding to a 1-water-layer complex in the interlayer.

## DISCUSSION

The results of this study give insights into the dynamic evolution of the Na-smectite-water system from a water-dominated to an air-dried stage (28–47% relative humidity). They also underline the large dependence of this evolution on the initial conditions present within the system. The three datasets in this work have distinctive features produced by the following variables: initial water/smectite ratio, stirring (or not) of the smectite-water system and ambient relative humidity. It is likely that the most important factor that these variables affect is the mobility of water molecules which in turn affects the readjustment ability of the smectite layers when relative humidity changes (see discussion below).

The smectite layers in dataset 1 were initially completely dispersed in water, with no long-range order. The layers were moving relatively freely in the water with only small groups of them becoming parallel or semi-parallel to each other at any one instant. The distances between the layers were very variable (Figure 5, 0–5 min), although most of them had a *d* value of ~12 Å. The interlayer spacings that formed did not cause the layers to come into fixed register. Instead, the system should be seen as consisting of dispersed

https://doi.org/10.1346/CCMN.2004.0520204 Published online by Cambridge University Press

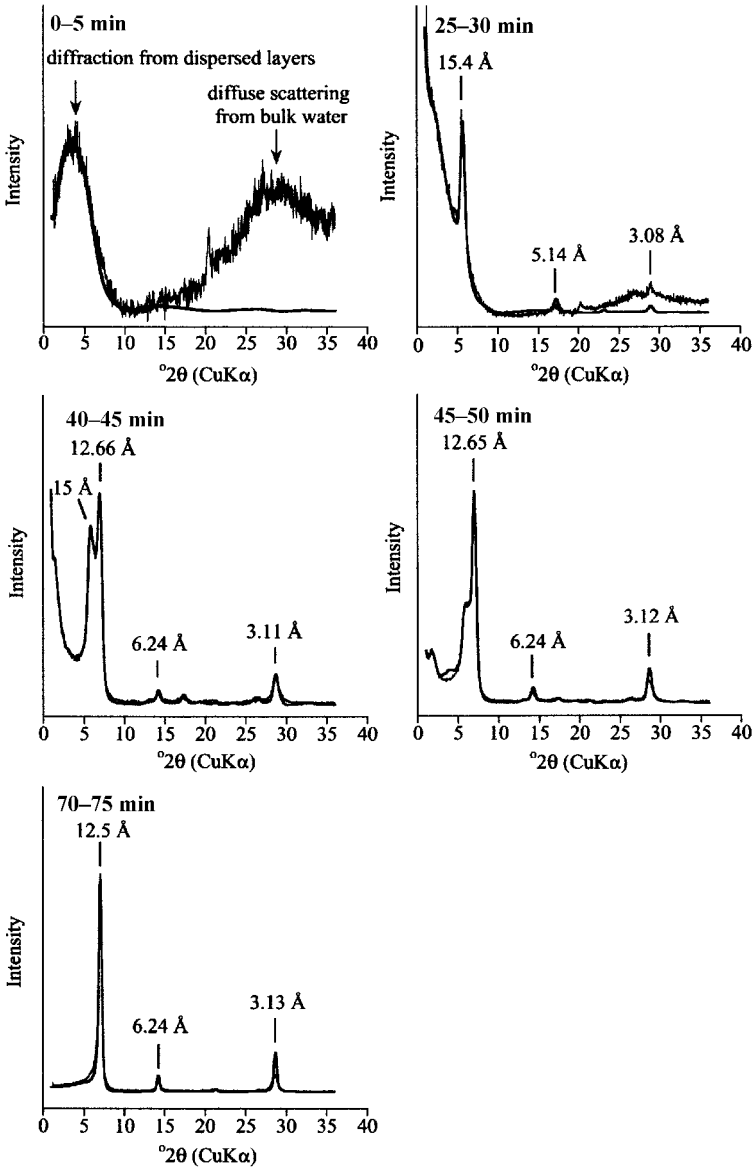


Figure 4. Measured and NEWMOD-simulated XRD patterns of Na-smectite at key stages of dehydration (dataset 1).

layers that moved relative to each other. Then, the distribution of *d* values in the water-dispersed particles changed from having an exponential-like to a Gaussian-like shape and some particles sedimented onto the substrate with a distinct *d* value of 15.4 Å (Figure 5, 25–30 min). Note that Figure 5 shows number of particles, not number of layers. The sedimented particles had a much larger number of layers than the water-dispersed ones (Table 1). In the 25–30 min plot, 16% of the layers are sedimented. In the 25–30 min pattern, the amount of evaporated water is negligible because the intensity of the diffuse water-scattering is the same as that seen on the 0–5 min pattern.

As evaporation and sedimentation continued, the distribution of smectite *d* values in the water-dispersed particles varied as indicated by the erratic trend of the low-angle maximum which had successive values of 48, 34, 63 and 39 Å. A small fraction of this erratic behavior is caused by the constant change of the background intensity which alters the apparent value of the diffraction maximum by between 0 and 5 Å, as measured after background subtraction. For the 40–45 min pattern, the simulated distribution of water-dispersed particles has a flat, Gaussian-like shape with a maximum at ~45 Å, spanning from 35 to 60 Å. In the following pattern (45–50 min), the maximum was observed at 52 Å and the calculated distribution of *d* values is similar although the total % values are lower. Therefore, the calculated patterns indicate that water-dispersed particles tended to have an increased average layer-separation as dehydra-

https://doi.org/10.1346/CCMN.2004.0520204 Published online by Cambridge University Press

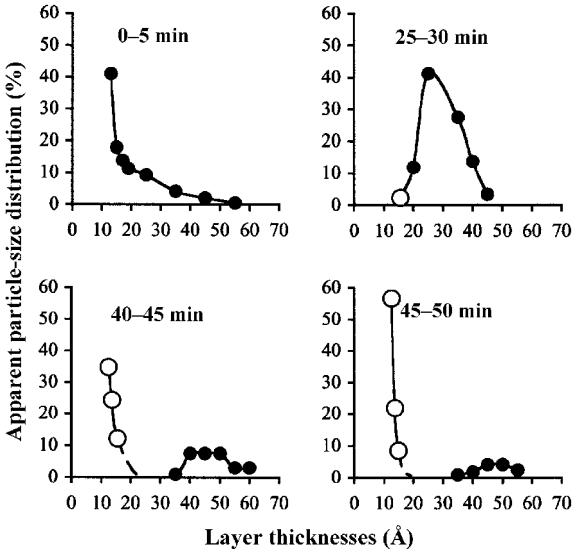


Figure 5. Apparent relative proportions of particle *d* values during Na-smectite dehydration derived from NEWMOD simulations of dataset 1. Filled circles denote water-dispersed particles, open circles denote deposited smectite crystallites.

tion proceeded. The water content in the 40–45 and 45–50 min patterns was substantially lower than in the initial patterns, but was sufficient to expand the few remaining dispersed layers to large *d* values. Notice that transforming the particle % values in the 40–45 and 45–50 min plots into layer % (by multiplying the number of particles by the average number of layers per particle) indicates that the relative proportion of dispersed to sedimented layers was negligible.

At this point, it is necessary to comment on the nature of the 'water-dispersed' particles. In the first part of the dataset, the water content was sufficient to maintain a population of physically dispersed smectite layers. However, after 35–40 min, the amount of water was too low to hold a dispersion and from this point onwards, the 'water-dispersed' particles should be considered as highly expanded layers with variable orientation with respect to both the sample substrate and each other. A simplified interpretation can be given to account for the evolution of the apparent *d* value distribution of the 'water-dispersed' particles. While the system was water-dominated, sedimentation of smectite with low *d* values (relative to the complete range observed here) expelled water molecules from these interlayers and became available to enter the interlayer region of highly expanded layers. This process was faster than water evaporation, and controlled the behavior of the water-dispersed particles. After ~35 min, the system became solid dominated. Water molecules were confined to the smectite surfaces and were no longer able to migrate from collapsing interlayers to become part of the dispersed particle population. After this, the highly expanded particles lost water progressively and more or less uniformly (as suggested by the similar *d* values distributions at 40–45 and 45–50 min in Figure 5) through evaporation, and became increasingly parallel to the previously dehydrated particles as they became part of their population. In addition to water mobility, the process will also be affected by other factors, such as hysteresis in hydration reactions, interlayer attraction-repulsion and creation of time-dependent 3-D structures, but very little is known about these. However, the transition from the *d* value distribution in the 0–5 min pattern to that in the 25–30 min pattern cannot be explained only by the diluting effect of the water expelled from shrinking interlayers, because in the 0–5 min pattern, most of the particles have a *d* value of only ~12 Å and have no excess interlayer water to expel. In this case, the change in *d*-spacing distribution may be aided by the reorganization of the water-smectite system by the creation of gel-like structures that are known to develop with time in undisturbed clay suspensions.

The interpretation of the evolution of the sedimented particles is more straightforward. The first stable crystallites had a 2-water-layer configuration. Between 0 and 30 min, a large continuum of *d* values existed for water-dispersed particles, as layers were undergoing sedimentation (15.4 to 60 Å). The lack of particles with *d* values of 15.4–35 Å may be attributed to two factors. Firstly, the transition of layer spacings from 15.4 to 35 Å could have been rapid so that intermediate layer spacings were not observed. Secondly, the dehydration of layers at this stage could be very inhomogeneous, causing layer deformation and inhibiting coherent basal diffraction. The 15.4 Å layers dehydrated progressively, generating one or more intermediate *d* values up to the final stable state of 12.5 Å. The need for a peak at 13.6 Å in pattern simulations indicates the existence of these transient intermediate stages. Although they were simulated with only one peak, more layer spacings may have been present. However, these are much less stable than the 15.4 and 12.5 Å smectite-water complexes. The rationality of the 001 series and the relatively large scattering domain sizes (Table 1) indicate that these *d* spacings were relatively homogeneous across numerous layers.

The most novel results in this work correspond to the water-dominated stages of the smectite-water system. There is very little information on this system in the literature. DiMasi *et al.* (2001) performed a synchrotron XRD analysis of water-dispersed Na-smectite in a static system, *i.e.* the water content was constant (smectite suspension held in a closed glass tube) and the sample was analyzed a few days after the suspension was prepared, so that short-term smectite-water structural rearrangements would have ceased prior to analysis. Their system had three strata: clear water at the top, a gel in the middle and a sediment at the bottom. The XRD patterns of the two lower strata were similar to the 25–30 min pattern in this work, with prominent diffuse scattering from water and a sharp peak at 15.0 Å.

https://doi.org/10.1346/CCMN.2004.0520204 Published online by Cambridge University Press

DiMasi *et al.* (2001) did not mention the inflection point that is observed in the rising background in the 25–30 min pattern (*i.e.* the diffraction maximum generated by the water-dispersed particles) and it is difficult to determine whether or not this feature is present in their pattern (Figure 1, DiMasi *et al.*, 2001), or even whether their low-angle cut-off is too high to show this feature. DiMasi *et al.* (2001) analyzed the orientation of smectite layers in their system and found that the layers in the lower stratum were oriented horizontally, as expected. However, the layers in the middle, gel-like stratum were strongly oriented in a vertical position (horizontal *c* axis). It is difficult to assess how their gel-like material could be related to the water-dispersed smectite layers investigated in this work. Both materials are above the sedimented layers, but in our work, the system was undergoing a rapid change whereas their system had reorganized substantially and reached a more stable state (although they reported appreciable changes after months). The vertical orientation of smectite layers in their gel-like material seems to contradict our assumption that water-dispersed layers would acquire a progressively increasing horizontal orientation but the differences between the experimental conditions of the two systems preclude further discussion. In addition, DiMasi *et al.* (2001), used NaCl (0.0001–0.012 M) solutions for their dispersions, as opposed to deionized water such as that used in this work ($<1 \times 10^{-6}$ M total electrolyte concentration). Such differences in electrolyte concentration may also be responsible for the different particle orientation because electrolyte concentration influences the 3-D arrangement of smectite layers.

The dehydration of a smectite slurry (dataset 2, Figure 2) evolved in a different way. Bragg diffraction from dispersed layers (55–35 Å) was observed as in dataset 1, but was present from the beginning of the experiment and was of a higher intensity, probably because a greater proportion of layers were in the highly-expanded state, or the orientation of layers was more parallel. The slurry experiment also produced 3-water-layer smectite. This is often absent in experiments reported in the literature and its appearance (unlike that of 1- and 2-water-layer smectite) seems to be largely dependent upon experimental conditions and procedures. Moore and Hower (1986) observed a peak above 18 Å in Na-smectite experiments under set humidity conditions. Collins *et al.* (1992) detected a short-lived 20.0 Å peak using neutron diffraction during dehydration of Na-smectite as the chamber containing the sample was evacuated. MacEwan and Wilson (1980) report several XRD studies of Na-smectite hydration and dehydration where this peak is observed only in two cases out of five, at 18.8 and 19.0 Å. In all these studies, the 18–20 Å peak was observed near 100% relative humidity. However, Yamada *et al.* (1994) and da Silva *et al.* (2002) did not observe this peak although they reached 100% or near 100% relative humidity conditions in their experiments. These differences may be due to variability in the nature of the different samples used in the experiments. However, the results of the experiments conducted in this study, show that even the same sample can behave differently depending on how the experiments are conducted. Although the 3-water-layer configuration is often not observed, computer simulations show that it is stable under certain conditions (Chang *et al.*, 1995; Karaborni *et al.,* 1996).

The low intensities of the 55, 35 and 18 Å peaks in dataset 3 (re-wetted thin film) indicate that the lack of stirring resulted in less water penetration into the smectite interlayers (few layers expanded above 15 Å) compared to datasets 1 and 2. In the slurry experiment, the presence and persistence of all the water configurations was probably facilitated by low water mobility so that water could only be removed from smectite interlayers by diffusing out to the edges of layers and evaporating. In the suspension experiment (dataset 1), the excess water initially present promoted the free evolution of the system, such that the higher-stability 1- and 2-water-layer configurations were favored over the very large layer-spacings and the 3-water-layer configuration.

The final state of the smectite in the dispersion experiment (dataset 1) showed a rational 00*l* series, indicating that it was a very homogeneous system, in which all layers had the same $d_{001}$ value. The slurry and the re-wetted film did not have rational 00*l* series and the peaks increased in width from 002 to 004, with the latter peak having a flat top in the slurry experiment. This peak broadening and displacement was caused by the presence of various hydration states that became more apparent in the high 00*l* peaks, where the corresponding diffraction maxima are better resolved. Also, a small amount of mixed-layering of different hydration states may have been present. The range of positions of the 004 peaks indicates an approximate *d* value range of 12.6–12.36 Å for the layer spacing. In contrast, the positions of the 001 peaks indicate a mean *d* value of 12.4 Å for this structure. Heterogeneous spacing of Na-smectite-water systems has been reported by other authors (*e.g.* Cases *et al.*, 1992), usually involving random mixed-layering of the several hydration states. The cause of this heterogeneity is variable layer charge. In this work, the relative humidity during the dispersion experiment was higher (47%) than that during the other experiments (28–30%). This is probably the cause of the different results because some high-charge layers may have had lower water contents at 28–30% relative humidity than at 47%. However, additional factors such as the attainment of complete dispersion, the rate of dehydration or dehydration duration may also play a role. A special case of heterogeneous *d* values is the ordered interstratification of alternating dehydrated (9.6 Å) and 12.4 Å layers reported by Moore and Hower (1986) from 65 to 12% relative humidity. It is

https://doi.org/10.1346/CCMN.2004.0520204 Published online by Cambridge University Press

possible that some of the layers in the slurry (dataset 2) and re-wetted thin-film (dataset 3) experiments have this arrangement, but the XRD patterns obtained in this work do not have a superstructure peak as in Moore and Hower's study and the position of the 001 peak is 11.2 Å rather than 12.4 Å. In addition, their experimental conditions were different to those in this study in that they stabilized their samples under various relative humidity conditions for 24 h prior to XRD analysis. This further emphasizes the influence that experimental conditions and procedures have on smectite hydration states.

## CONCLUSIONS

(1) *In situ* XRD-PSD techniques detect rapid structural rearrangement processes that evolve during the dehydration of smectite, because the static experimental geometry permits the study of water-dominated systems with fast data collection over a very large range of 2θ. Whole-profile modeling of the diffraction patterns is necessary in order to interpret properly the diffraction behavior of multiple-layer and mixed-layer particles in smectite-water systems.

(2) The behavior of Na-smectite during dehydration is dependent upon experimental conditions. In this work, the following variables affected the structural rearrangement during dehydration: water/smectite ratio, attainment of complete smectite dispersion, and atmospheric relative humidity. Other variables such as layer charge, layer-charge location (octahedral *vs.* tetrahedral) and layer-charge heterogeneity should also be considered when comparing different smectite types.

(3) During Na-smectite dehydration, two populations of layer systems were observed: layers stacked in well developed crystallites and those highly expanded with a low degree of mutual orientation.

(4) Well developed crystallites had two favored arrangements with $d_{001}$ values of 15.4 and 12.5 Å, and a less favored arrangement with a $d$ value of 18.5 Å, the occurrence of which depended upon experimental conditions.

(5) The layer separation in highly expanded layers was very variable and changed during dehydration, with a tendency to become larger as dehydration of the system proceeded.

(6) The existence of transient structures between those corresponding to 15.4 and 12.5 Å was observed as XRD intensity at intermediate positions between these two peaks, which was made apparent in the pattern modeling. The same may be true between 18.5 and 15.4 Å, although this was not investigated by modeling. No intermediate $d$ values were observed between the highly expanded layers and the well-developed crystallites in the final stages of dehydration, indicating that this was a very rapid and/or a very irregular process that disrupted coherent XRD.

## ACKNOWLEDGMENTS

The authors are very grateful to N. Güven, D. Eberl and R. Ferrell for their useful suggestions and comments. Part of this work was completed by J.W. during a NERC-funded (UK) PhD studentship.

## REFERENCES

Batchelder, M. and Cressey, G. (1998) Rapid, accurate phase quantification of clay-bearing samples using a position-sensitive X-ray detector. *Clays and Clay Minerals*, **46**, 183–194.

Bergaya, F. and Vayer, M. (1997) CEC of clays: measurement by adsorption of a copper ethylenediamine complex. *Applied Clay Science*, **12**, 275–280.

Blanton, T.N., Huang T.C., Toraya, H., Hubbard, C.R., Robie, S.B., Louër, D., Göbel, H.E., Will, G., Gilles, R. and Raferty, T. (1995) JCPDS – International Centre for Diffraction Data round robin study of silver behenate. A possible low-angle X-ray diffraction calibration standard. *Powder Diffraction*, **10**, 91–95.

Boek, E.S., Coveney, P.V. and Skipper, N.T. (1995a) Monte Carlo molecular modeling studies of hydrated Li-, Na-, and K-smectites: Understanding the role of potassium as a clay swelling inhibitor. *Journal of the American Chemical Society*, **117**, 12608–12617.

Boek, E.S., Coveney, P.V. and Skipper, N.T. (1995b) Molecular modeling of clay hydration: A study of hysteresis loops in the swelling curves of sodium montmorillonites. *Langmuir*, **11**, 4629–4631.

Bradley, W.F., Grim, R.E. and Clark, G.L. (1937) A study of the behaviour of montmorillonite upon wetting. *Zeitschrift Kristallographie*, **A97**, 216–222.

Brindley, G.W. (1980) Quantitative X-ray mineral analysis of clays. Pp. 411–438 in: *Crystal Structures of Clay Minerals and their X-ray Identification* (G.W. Brindley and G. Brown, editors). Monograph **5**, Mineralogical Society, London.

Cases, J., Bérend, I., Besson, G., François, M., Uriot, J.P., Thomas, F. and Poirier, J.E. (1992) Mechanism of adsorption and desorption of water vapor by homionic montmorillonite. 1. The sodium-exchanged form. *Langmuir*, **8**, 2730–2739.

Chang, F-R.C., Skipper, N.T. and Sposito, G. (1995) Computer simulation of interlayer molecular structure in sodium montmorillonite hydrates. *Langmuir*, **11**, 2734–2741.

Chatterjee, A., Iwasaki, T., Ebina, T. and Miyamoto A. (1999) A DTF study on clay-cation-water interaction in montmorillonite and beidellite. *Computational Materials Science*, **14**, 119–124.

Collins, D.R., Fitch, A.N. and Catlow, R.A. (1992) Dehydration of vermiculites and montmorillonites: A time-resolved powder neutron diffraction study. *Journal of Materials Chemistry*, **2**, 865–873.

da Silva, G., Fossum, J., DiMasi, E., Måløy, K. and Lutnæs, S. (2002) Synchrotron X-ray scattering studies of water intercalation in a layered synthetic silicate. *Physical Review E*, **66**, 011303-1–011303-8.

DiMasi, E., Fossum, J., Gog, T. and Venkataraman, C. (2001) Orientational order in gravity dispersed clay colloids: A synchrotron X-ray scattering study of Na fluorohectorite suspension. *Physical Review E*, **64**, 061704-1–061704-7.

Glaeser, R. and Méring, J. (1968) Homogeneous hydration domains of the smectites. *Comptes Rendus de Seances de l'academie des sciences, Paris*, **267**, 436–466.

Howard, S.A. and Preston, K.D. (1989) Profile fitting of powder diffraction patterns. Pp. 217–276 in: *Modern Powder Diffraction* (D.L. Bish and J.E. Post, editors).

Reviews in Mineralogy, **20**. Mineralogical Society of America, Washington, D.C.

Karaborni, S., Smit, B., Heidug, W., Urai, J. and van Oort, E. (1996) The swelling of clays: molecular simulations of the hydration of montmorillonite. *Science*, **271**, 1102–1104.

Kawamura, K., Ichikawa, Y., Nakano, M., Kitiyama, K. and Kawamura, H. (1999) Swelling properties of smectite up to 90ºC. In-situ X-ray diffraction experiments and molecular dynamic simulations. *Engineering Geology*, **54**, 75–79.

Keren, R. and Shainberg, I. (1975) Water vapor isotherms and heat of immersion of Na/Ca montmorillonite systems – 1: homoionic clay. *Clays and Clay Minerals*, **23**, 193–200.

MacEwan, D.M.C. and Wilson, M.J. (1980) Interlayer and intercalation complexes of clay minerals. Pp. 197–248 in: *Crystal Structures of Clay Minerals and their X-ray Identification* (G.W. Brindley and G. Brown, editors). Monograph **5**, Mineralogical Society, London.

Moore, D.M. and Hower, J. (1986) Ordered interstratification of dehydrated and hydrated smectite. *Clays and Clay Minerals*, **34**, 379–384.

Moore, D.M. and Reynolds, R.C. (1997) *X-ray Diffraction and the Identification and Analysis of Clay Minerals.* Oxford University Press, Oxford, UK.

Reynolds, R.C., Jr. and Reynolds, R.C., III (1996) *NEWMOD: The Calculation of One-Dimensional X-ray Diffraction Patterns of Mixed-Layered Clay Minerals. Computer Program.* 8 Brook Road, Hanover, New Hampshire, USA.

Skipper, N.T., Refson, K. and McConnell, J.D.C. (1991) Computer simulation of interlayer water in 2:1 clays. *Journal of Chemical Physics*, **94**, 7434–7445.

Skipper, N., Chang, F.-R. and Sposito, G. (1995) Monte Carlo simulation of interlayer molecule structure in swelling clay minerals. 1. Methodology. *Clays and Clay Minerals*, **43**, 285–293.

Sposito, G., Park, S.-H. and Sutton, R. (1999) Monte Carlo simulation of the total radial distribution function for interlayer water in sodium and potassium montmorillonites. *Clays and Clay Minerals*, **47**, 192–200.

Yamada, H., Nakazawa, H., Hashizume, H., Shimomura, S. and Watanabe, T. (1994) Hydration behavior of Na-smectite crystals synthesized at high-pressure and high-temperature. *Clays and Clay Minerals*, **42**, 77–80.

(*Received 13 May 2003; revised 22 October 2003; Ms. 791; A.E. Ray E. Ferrell*)